Multi-slice Tomographic Reconstruction: To Couple or Not to Couple

Preeti Gopal*
ViGIL, Department of Computer Science and Engineering, Indian Institute of Technology Bombay &
IITB-Monash Research Academy
preetig@cse.iitb.ac.in

Sharat Chandran
ViGIL, Department of Computer Science and Engineering, Indian Institute of Technology Bombay
sharat@cse.iitb.ac.in

Imants Svalbe
Department of Physics and Astronomy, Monash University
imants.svalbe@monash.edu

Ajit Rajwade
ViGIL, Department of Computer Science and Engineering, Indian Institute of Technology Bombay
ajitvr@cse.iitb.ac.in

ABSTRACT

Recent work in tomography focuses on algorithms that enable faster and more accurate reconstruction from as few measurements as possible. We review the advantage of jointly reconstructing multiple slices and show that joint reconstruction may suffer in the presence of adjacent dissimilar slices. This gives rise to the need to detect similarity or dissimilarity of unknown images before performing joint reconstruction.

We propose a method to detect 'similar' slices *directly from their tomographic measurements* and juxtapose these similar slices. Since the images themselves are not available by definition, we compute similarity between slices based on *image moments*; these in turn are estimated in a novel way from Radon projection moments. A segmented least squares algorithm is then designed to couple only similar slices. Our results confirm the benefit of this method for tomographic reconstruction.

Keywords

Compressive sensing, Radon projection moments, image moments, tomographic reconstruction

1. INTRODUCTION

Research in tomographic reconstruction is driven by the need to speed up the acquisition process. This can be done by reducing the number of measurements, which at first glance, might also result in the reduced quality of reconstruction. However, recent developments in *compressive sensing* [8, 7] enable reconstruction from measurements fewer than that specified by the Nyquist criterion.

Since tomography involves multiple measurements of slices in a 3D volume, a related idea in the compressive sensing framework is to solve for the complete reconstruction of several slices in a batch. Several slices may individually have a small number of measurements, but together, they may carry more information. The solutions are in an iterative

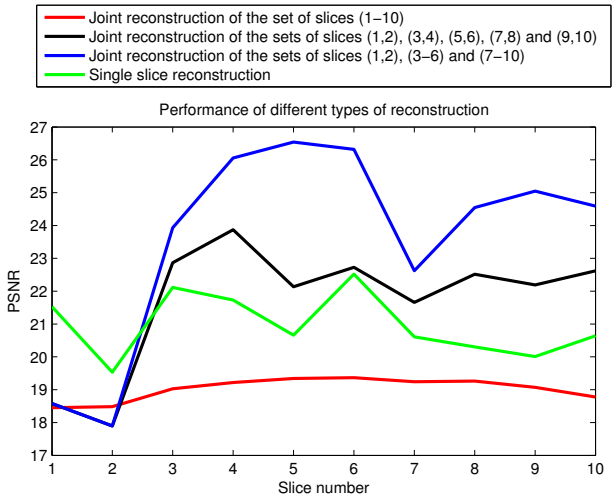

(a)

Figure 1: With every combination of sets of coupled slices, we get a different performance in joint reconstruction. The method in this paper determines the best coupling mechanism.

*Corresponding author

ICVGIP, December 18-22, 2016, Guwahati, India

DOI: http://dx.doi.org/10.1145/3009977.3010054

framework of an optimization problem using the sparsity of the underlying data under a suitable basis. As a result modern methods strive to use a large number of slices to obtain better quality results.

A practical problem in this is in the determination of the number of slices to jointly solve for, in the reconstruction. Fig. 1 (reconstructions on 10 slices of humerus bone CT [2]) throws some light on this situation. We see that at one extreme we can use one slice at a time and reconstruct. However, using different combinations of (multiple) slices results in better quality as can be seen in the PSNR plot. That said, using a very large number of slices actually hurts the reconstruction. We therefore need a systematic procedure to choose the best coupling of slices for each dataset, and couple only 'similar' slices. This is vexing because we don't have the true slices in the first place, and therefore it's not clear whether a slice is similar to another slice to determine coupling. In this paper, we determine the best coupling in a compressive sensing framework, and hence we review related definitions.

1.1 Terminology in Compressive Sensing

Let $\boldsymbol{x} \in \mathbb{R}^n$ be the original signal, and $\boldsymbol{\Phi} \in \mathbb{R}^{m \times n}$ be the measurement matrix that produces a measurement vector $\mathbf{y} = \boldsymbol{\Phi}\mathbf{x}$ where $\mathbf{y} \in \mathbb{R}^m$, $m \ll n$. Let $\boldsymbol{\Psi}$ be the sparse representation matrix for $\mathbf{x}$, i.e., $\mathbf{x} = \boldsymbol{\Psi}\boldsymbol{\theta}$ where $\boldsymbol{\theta} \in \mathbb{R}^n$ is a sparse or compressible vector. Now we have

$$\mathbf{y} = \boldsymbol{\Phi}\boldsymbol{\Psi}\boldsymbol{\theta} + \boldsymbol{\eta} \tag{1}$$

where $\boldsymbol{\eta}$ is the measurement noise such that $\|\boldsymbol{\eta}\|_2 \leq \epsilon$ where $\epsilon \geq 0$ is an upper bound on the magnitude of noise. Then $\boldsymbol{\theta}$ can be estimated by solving

$$\hat{\boldsymbol{\theta}} = \text{argmin}||\boldsymbol{\theta}||_1 \text{ such that } ||\mathbf{y} - \boldsymbol{\Phi}\boldsymbol{\Psi}\boldsymbol{\theta}||_2 \leq \epsilon. \tag{2}$$

As per [7], the estimate of $\hat{\boldsymbol{\theta}}$ obeys

$$||\hat{\boldsymbol{\theta}} - \boldsymbol{\theta}||_2 \leq C_0||\boldsymbol{\theta} - \boldsymbol{\theta}_s||_1/\sqrt{s} + C_1\epsilon \tag{3}$$

where $\boldsymbol{\theta}_s$ is a vector with the s largest coefficients in $\boldsymbol{\theta}$ alone, in terms of absolute value (and the rest set to 0). Thus the error is bound by the sum of two terms: the first one proportional to the estimation error in the noiseless case, and the other proportional to the noise magnitude. The coefficients C_0 and C_1 are independent of n and are generally small, being proportional to the incoherence between $\boldsymbol{\Psi}$ and $\boldsymbol{\Phi}$. Hence, this technique is robust to noise. Also note that, the minimum number of measurements required m is related to the reconstruction quality by:

$$m \geq C \log(n/\delta)\ ||\boldsymbol{\theta}||_0\ \mu^2(\boldsymbol{\Psi}, \boldsymbol{\Phi}) \tag{4}$$

where $\mu^2(\boldsymbol{\Psi}, \boldsymbol{\Phi})$ is the level of coherency between $\boldsymbol{\Psi}$ and $\boldsymbol{\Phi}$. This also shows that as $\boldsymbol{\theta}$ becomes less sparse, more measurements have to be taken [6]. [18] aims to reduce m, the number of measurements required, by increasing the sparsity of $\boldsymbol{\theta}$.

1.2 Related Work & Problem Definition

In several applications involving tomographic reconstruction, the aim is to reconstruct multiple consecutive 2D slices from a 3D volume (hereafter simply called *slices*), or to reconstruct a single 2D slice as it evolves over time (hereafter referred to as *time-frames*). There has been a lot of recent work [16],[15],[5],[17] in joint reconstruction of multiple MRI slices/time-frames. However, all of these assume that consecutive slices/time-frames are *always* similar. In [16], successive 2D slices are jointly represented using 3D wavelet transforms. In [15], the first time frame is densely sampled; the support of its wavelet coefficients is identified and knowledge of this support is used to reconstruct all consecutive frames. In [5], each time frame is first independently reconstructed using 2D wavelet sparsity. This is followed by a motion estimation step, and then a motion compensation step where all frames are re-estimated using the fact that the difference between a frame and its motion-compensated successive frame is sparse. In [17] a transform basis, the Kronecker product of a 2D Wavelet (for spatial dimensions) and a 1D Fourier for the temporal direction, has been used where the latter sparsely represents periodic motion.

In contrast to all work mentioned above, we do not assume successive slices or time-frames to be always similar, nor do we assume periodicity as in [17]. We allow for cases where there could be significant differences between a set of consecutive slices (say at the boundary of an object). Fig. 2 shows that joint reconstruction is not always superior. Visual result of reconstruction of one of the slices can be seen in Fig. 3

1.3 Contributions

Our key contributions in this work are:

- The idea of using image moments as a measure of similarity of underlying slices. Note that Radon projections are acquired at different set of angles for each slice, and therefore, one cannot compare them directly to deduce similarity of the underlying data. Using a different set of angles for different slices is critical in the compressive sensing framework. For example, for adjacent slices, this enables us to capture nearly twice the information for a pair of slices, when jointly reconstructed.

- A scheme for best coupling of slices after similarity, or lack thereof, is deduced.

- Verification of the proposed procedure by carrying out experiments on multiple datasets of different domains (both medical and non-medical) (these will be made available in the public domain).

Governing scheme: Let the measured data at time t be given by $\mathbf{y}_t = \boldsymbol{\Phi}_t\mathbf{x_t} = \boldsymbol{\Phi}_t\boldsymbol{\Psi}\boldsymbol{\theta}_t$, where $\boldsymbol{\Phi}_t$ is the measurement matrix at time t. Let $\mathbf{R}_t = \boldsymbol{\Phi}_t\boldsymbol{\Psi}$. Then, the measurements of any two consecutive frames are expressed [18] as

$$\begin{aligned}\begin{bmatrix}\mathbf{y}_t \\ \mathbf{y}_{t+1}\end{bmatrix} &= \begin{bmatrix}\mathbf{R}_t & \mathbf{0} \\ \mathbf{0} & \mathbf{R}_{t+1}\end{bmatrix}\begin{bmatrix}\boldsymbol{\theta}_t \\ \boldsymbol{\theta}_{t+1}\end{bmatrix} + \begin{bmatrix}\boldsymbol{\eta}_t \\ \boldsymbol{\eta}_{t+1}\end{bmatrix} \\ &= \begin{bmatrix}\mathbf{R}_t & \mathbf{0} \\ \mathbf{R}_{t+1} & \mathbf{R}_{t+1}\end{bmatrix}\begin{bmatrix}\boldsymbol{\theta}_t \\ \Delta\boldsymbol{\theta}_t\end{bmatrix} + \begin{bmatrix}\boldsymbol{\eta}_t \\ \boldsymbol{\eta}_{t+1}\end{bmatrix}\end{aligned}$$

where $\Delta\boldsymbol{\theta}_t = \boldsymbol{\theta}_{t+1} - \boldsymbol{\theta}_t$. Since adjacent frames often have a significant amount of redundancy, $\Delta\boldsymbol{\theta}_t$ is also sparse and infact more sparse than $\boldsymbol{\theta}_t$ and $\boldsymbol{\theta}_{t+1}$. In this technique, both $\boldsymbol{\theta}_t$ and $\Delta\boldsymbol{\theta}_t$ are estimated by solving the following:

$$\begin{bmatrix} \hat{\boldsymbol{\theta}}_t \\ \Delta\hat{\boldsymbol{\theta}}_t \end{bmatrix} = \underset{\boldsymbol{\theta},\Delta\boldsymbol{\theta}}{\operatorname{argmin}} \left\| \begin{bmatrix} \mathbf{y}_t \\ \mathbf{y}_{t+1} \end{bmatrix} - \begin{bmatrix} \mathbf{R}_t & \mathbf{0} \\ \mathbf{R}_{t+1} & \mathbf{R}_{t+1} \end{bmatrix} \begin{bmatrix} \boldsymbol{\theta}_t \\ \Delta\boldsymbol{\theta}_t \end{bmatrix} \right\|_2^2 + \tau \left\| \begin{bmatrix} \boldsymbol{\theta}_t \\ \Delta\boldsymbol{\theta}_t \end{bmatrix} \right\|_1 \quad (5)$$

In [18], this method was extended to jointly reconstruct more frames. A maximum of four frames were taken together due to constraints in memory and the time taken to compute one optimization pass. The disadvantage of such a coupling is that if the frames were dissimilar (for example, across video shot boundaries), the differences between their coefficients will no longer be sparse, requiring more measurements. *We present a method to first verify whether successive time-frames or slices are similar, and only then decide whether to couple them.*

2. METHOD

Hereafter, we have used the terms 'slice'(2D cross-sections across depth of an object) and 'time-frame' interchangeably as our algorithm is applicable for both the cases. We chose our measurement matrix $\mathbf{\Phi}$ to represent the Radon transform, which is quite natural for CT. However, our method is equally applicable for radial sampling strategies in MRI as well (where the acquisition involves sampling the Fourier space of the object being scanned). This is because, if radial sampling were used for MRI, the Fourier Slice Theorem can directly relate the Fourier coefficients along radial lines in 2D Fourier space of the object to the Fourier transform of the Radon projections along the corresponding orientations. Although other sampling patterns like spiral and uniform sampling in Cartesian grid is possible in MRI, the radial pattern has the advantage that it enables dense sampling in the low frequency region which has higher information content. Further, we chose the sparse representation matrix $\mathbf{\Psi}$ to be the Discrete Cosine Transform (DCT).

2.1 Reconstruction using Successive Slice Redundancy

Given the choice of $\mathbf{\Phi}$ and $\mathbf{\Psi}$, for each set of slices that will be reconstructed jointly, we use a different set of angles while taking Radon measurements. This enables us to capture more information as the slices are expected to be similar. For example, if slice 1 is measured with v views and slice 2 is measured with a different set of v views, then together we have information from $2v$ views for joint reconstruction of each slice. This is why the reconstruction quality is expected to improve. Our aim is to couple as many similar slices as possible. *However, if we couple dissimilar frames, then the quality of reconstruction will deteriorate because the difference between two different s-sparse vectors could be as high as $2s$-sparse — which will require more measurements to be captured.* This can be seen from our experiment with lumbar dataset [3] consisting of 12 slices where successive slices were significantly different (probably due to low depth resolution while acquisition). The joint reconstruction of all slices together gave the least PSNR as seen in Fig. 2. Visual result of the reconstruction of one of the slices can be seen in 3. Moreover, coupling a large number of slices also increases the computation time. Therefore, it is necessary to formulate a technique that provides us with sets of similar slices.

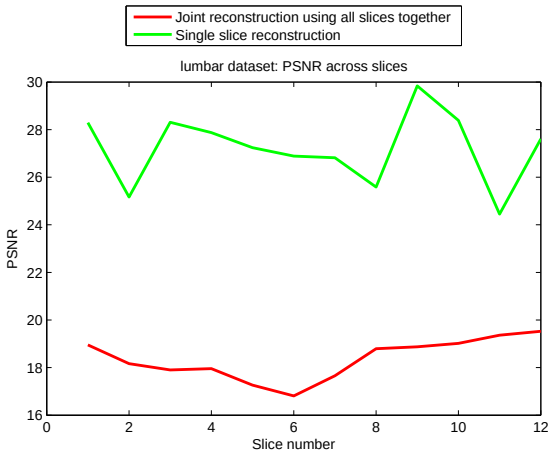

Figure 2: Reconstruction on dataset of the lumbar spine [3]: Joint reconstruction may actually hurt quality

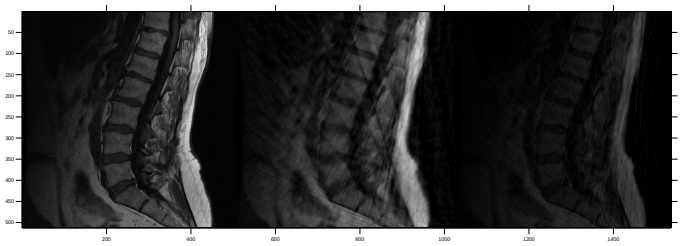

Figure 3: Reconstruction of (left) a slice of lumbar spine by (center) single slice reconstruction, (right) Joint reconstruction with all slices together

2.2 Computing Similarity between Slices

Since, to begin with we neither have the original slices nor their reconstructed versions, we need some metric that

- can be computed from the available tomographic measurements
- represents in some sense, the similarity between two slices

We choose this metric to be geometric image moments. Moments have, for long, been used to describe the shape of a set of points. An image, $f(x, y)$ can be uniquely expressed [11] by the set of all image moments. When all the image moments of two slices are almost equal, this implies that the images are very similar and hence the differences between their DCT coefficients will be sparse, which is favourable for reconstruction. Therefore, we take the differences in image moments between two slices as a measure of dissimilarity and then decide whether or not to couple those slices. Each geometric image moment is a weighted sum of the pixel intensities of an image. The image moment of order $p + q$ is given by [10]:

$$\mathrm{IM}_{\mathrm{p,q}} = \int_{-\infty}^{+\infty}\!\!\int \mathrm{f(x,y)}\ \mathrm{x^p}\ \mathrm{y^q}\,\mathrm{dx}\,\mathrm{dy}. \quad (6)$$

These can also be viewed as projection of a 2D function onto monomials. They are known to describe various image

properties. For example, the zeroth order moment represents the area of the image (sum of all pixel intensities in a binary image) and the first order moments represent the mean. The higher orders describe other features like the orientation of the pattern. Since we cannot obtain all the moments, we compute a few of them from the Radon projection moments [19]. The k^{th} order Radon projection moment at an angle Θ is given by

$$\mathrm{PM}_{\Theta}^{(\mathrm{k})} = \int_{-\infty}^{+\infty} \mathrm{P}_{\Theta}(\mathrm{s})\mathrm{s}^{\mathrm{k}}\,\mathrm{ds} \tag{7}$$

where $P_{\Theta}(.)$ is the Radon projection measured at view Θ, and is given by

$$P_{\Theta}(s) = \iint_{-\infty}^{+\infty} f(x,y)\ \delta(x\cos\Theta + y\sin\Theta - s)\ dxdy \tag{8}$$

Therefore,

$$PM_{\Theta}^{(k)} = \iint_{-\infty}^{+\infty} f(x,y)\ (x\cos\Theta + y\sin\Theta)^k\ dxdy \tag{9}$$

And,

$$(x\cos\Theta + y\sin\Theta)^k = \sum_{l=0}^{k} \binom{k-l}{k} (x\cos\Theta)^{k-l}\ (y\sin\Theta)^l \tag{10}$$

Eq. 11 relates the image moments $\mathrm{IM}_{\mathrm{p,q}}$ of order $p+q$ of a slice with its k^{th} order projection moment $\mathrm{PM}_{\Theta}^{\mathrm{k}}$, with projections being taken at an orientation Θ [19].

$$\begin{pmatrix} \mathrm{IM}_{\mathrm{k},0} \\ \mathrm{IM}_{\mathrm{k}-1,1} \\ \vdots \\ \mathrm{IM}_{0,\mathrm{k}} \end{pmatrix} = \mathbf{C}^{-1} \begin{pmatrix} \mathrm{PM}_{\Theta_1}^{\mathrm{k}} \\ \mathrm{PM}_{\Theta_2}^{\mathrm{k}} \\ \vdots \\ \mathrm{PM}_{\Theta_{\mathrm{k}+1}}^{\mathrm{k}} \end{pmatrix} \tag{11}$$

where

$$\mathbf{C} = \begin{pmatrix} \cos^k\Theta_1 & \binom{k-1}{k}\cos^{k-1}\Theta_1\sin\Theta_1 & \dots & \sin^k\Theta_1 \\ \cos^k\Theta_2 & \binom{k-1}{k}\cos^{k-1}\Theta_2\sin\Theta_2 & \dots & \sin^k\Theta_2 \\ \vdots & \vdots & \dots & \vdots \\ \cos^k\Theta_{k+1} & \binom{k-1}{k}\cos^{k-1}\Theta_{k+1}\sin\Theta_{k+1} & \dots & \sin^k\Theta_{k+1} \end{pmatrix}$$

Thus, in order to compute image moments of order k, we need projections from at least $k+1$ views: $\Theta_1, \Theta_2 ... \Theta_{k+1}$. In our experiments, we have used image moments of order 5 and lower.[1]

2.3 Optimally Coupling Slices

Since the difference between two different s-sparse vectors is $2s$-sparse, we want to avoid joint reconstruction of dissimilar slices. We have used the segmented least squares algorithm [13] to optimally bunch together all consecutive similar slices. Let j through n (including n) be the last bunch of slices coupled for reconstruction. Then, the total minimal error in reconstructing all n frames can be seen as the sum of three terms: the minimum error in reconstructing the first $(j-1)$ slices, the error in joint reconstruction of slices j through n, and the penalty for the break at frame j, i.e., not coupling slices $j-1$ and j. Mathematically,

$$\mathrm{OPT(n)} = \min_{1\le \mathrm{j} \le \mathrm{n}} (\mathrm{e_{j,n}} + \mathrm{D} + \mathrm{OPT(j-1)}) \tag{12}$$

where, OPT(n) is the total error of reconstructing all n slices; $\mathrm{e_{j,n}}$ is the average difference in image moments between successive slices from slice j to n, including j and n; (this is an indicator of the error in joint reconstruction of slices j through n); and D is the penalty of introducing a break in coupling, between slice $j-1$ and j. D is an important model parameter in our optimality scheme. A high value will couple all slices even if they are dissimilar and a low value will mostly favor single slice reconstruction.

3. EXPERIMENTS AND RESULTS

We solve an unconstrained version of Eq. 2 as shown below:

$$\text{minimize } (||\boldsymbol{\Phi\Psi\theta} - \mathbf{y}||_2^2 + \lambda||\boldsymbol{\theta}||_1) \tag{13}$$

using an existing solver [14]. Eq. 13 is known as the L_1-regularized Least Squares problem [12]. From proposition 3.2 in [9], we know that the solution to Eq. 13 and Eq. 2 are equivalent. λ is the regularization parameter and its value is usually fixed on a trial and error basis. We fixed it to be 0.01. We performed experiments on different datasets and compared the following reconstruction techniques, using 2D-DCT as the sparse transform:

- Independent single-slice reconstruction,
- Joint reconstruction coupling each and every slice,
- Joint reconstruction with a scheme that involves a subset of all slices (coupling every two adjacent slices).
- Joint reconstruction coupling slices bunched together by our optimality scheme.

Since we have the ground truth slices, our quantitative evaluation of the reconstructed versions is based on Peak Signal to Noise Ratio (PSNR). It is defined as

$$\mathrm{PSNR} = 10\log_{10}\frac{\mathrm{I_{max}^2}}{\mathrm{MSE}} \tag{14}$$

where $\mathrm{I_{max}}$ denotes the maximum pixel intensity value in the entire slice; and MSE denotes mean squared error with respect to the reference ground truth slice.

3.1 Walnut dataset

We took 60 slices from a CT Walnut dataset [4]. Each slice was of size 240×240 and represented different axial depth. Radon measurements were taken along 20 angles (8.3% of the data is measured). Fig. 4 shows the PSNR plots after reconstruction. Independent single slice reconstruction was poor. The segmented least squares based method performed better in most slices, than joint reconstruction of all the slices. We have chosen D to be d times the average difference in image moments between consecutive slices, where $d = 1.45$. The segmented least squares algorithm coupled the slices in the following manner: (1-23), (24-27) and (31-60). All the remaining frames were not coupled and reconstructed as per single slice reconstruction.

[1]Thus, the following set of 21 moments were used in our experiments: {$\mathrm{IM_{0,0}}$, $\mathrm{IM_{0,1}}$, $\mathrm{IM_{1,0}}$, $\mathrm{IM_{2,0}}$, $\mathrm{IM_{0,2}}$, $\mathrm{IM_{1,1}}$, $\mathrm{IM_{0,3}}$, $\mathrm{IM_{3,0}}$, $\mathrm{IM_{1,2}}$, $\mathrm{IM_{2,1}}$ ... $\mathrm{IM_{5,0}}$, $\mathrm{IM_{0,5}}$, $\mathrm{IM_{3,2}}$, $\mathrm{IM_{2,3}}$, $\mathrm{IM_{1,4}}$ and $\mathrm{IM_{4,1}}$}.

3.2 Humerus dataset

We took 110 slices from a CT dataset of the Humerus bone [2]. Each slice was of size 160×160 and represented different axial depth. Radon projections were computed for 20 angles (12.5% of the data is measured)[2]). Fig. 5 shows the PSNR plots after reconstruction, and the visual results can be found in our supplementary material. As seen in Fig. 8, the reconstruction was poor when all the slices were coupled together. In most cases, the segmented least squares based coupled reconstruction performed better than single slice reconstruction. Although the performance using adjacent slice coupling is comparable to our proposed coupling method, this is not the case in other experiments. Further, there is no specific reason for choosing adjacent two-slice coupling over adjacent three-slice or four-slice coupling, or, for that matter, a mixture of these.

We have chosen D to be d times the average difference in image moments between consecutive slices, where $d = 1.3$. The segmented least squares algorithm coupled the slices in the following manner: (2-8), (10-18), (26-41), (45-67), (71-91) and (98-110). All the remaining slices were not coupled and reconstructed as per single slice reconstruction.

3.3 Brainweb dataset

We took 60 slices from a Brainweb dataset [1]. Each slice was of size 180×180 and represented different axial depth. Radon measurements were taken along 25 angles (13.89% of the data is measured). Fig. 6 shows the PSNR plots after reconstruction and the visual results can be found in our supplementary material. As seen in Fig. 7, the reconstruction was poor when all the slices were coupled together. The segmented least squares based method performed better in most slices, than single slice reconstruction. We have chosen D to be d times the average difference in image moments between consecutive slices, where $d = 1.1$. The segmented least squares algorithm coupled the slices in the following manner: (6-18), (20-37), (43-46), (52-56) and (58-60). All the remaining frames were not coupled and reconstructed as per single slice reconstruction.

Note that in most datasets (and especially in Brainweb), the PSNR continuously decreases for the case of joint reconstruction with all slices. This is because the i^{th} slice is computed after reconstructing the DCT coefficients of all the previous slices, i.e.

$$\boldsymbol{\theta}_i = \boldsymbol{\theta}_{i-1} + \Delta\boldsymbol{\theta}_{i-1} \tag{15}$$

where $\Delta\boldsymbol{\theta}_{i-1} = \boldsymbol{\theta}_i - \boldsymbol{\theta}_{i-1}$. Hence, the reconstruction error adds up cumulatively and therefore PSNR decreases as i, the slice number, increases.

For all our experiments, the maximum number of permitted iterations in the *compressive sensing* solver was set to 500. Single slice reconstruction was the fastest of all techniques, taking less than a minute for each slice. As we couple more number of slices, the time taken for reconstruction increases. In general, we observed that if single slice method takes T units of time, then joint reconstruction of n slices takes higher than nT units of time.

[2]Percentage of data measured by taking k projections of a slice of size [sz sz] is approximately equal to $\frac{k \times sz}{sz \times sz} \times 100$

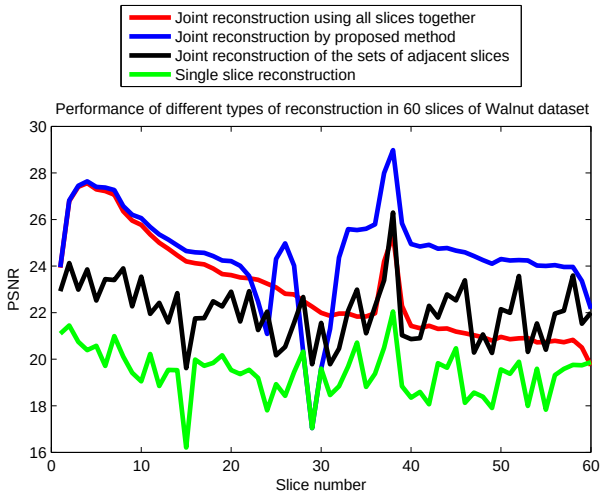

Figure 4: Reconstruction on the Walnut dataset [4]. Our method combines slices (1-23), (24-27) and (31-60)

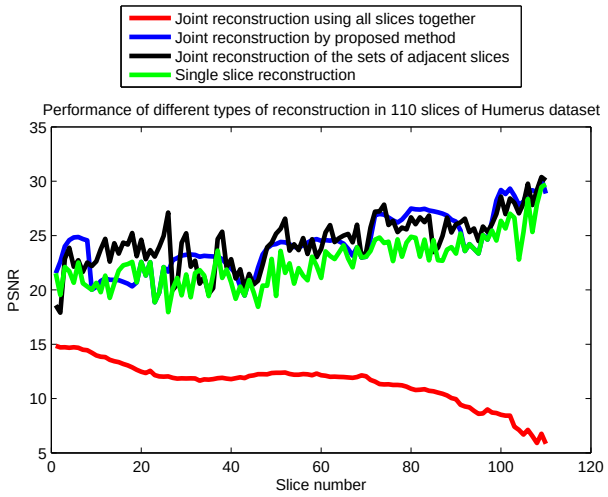

Figure 5: Reconstruction on the Humerus dataset [2]. Our method combines slices (2-8), (10-18), (26-41), (45-67), (71-91) and (98-110)

4. CONCLUSION

Although joint reconstruction by coupling many similar slices is useful, the reconstruction accuracy may degrade if dissimilar slices are coupled. We have proposed a new technique to compute similarity between slices directly from their tomographic measurements, and thereby encourage coupling of only the similar slices for joint reconstruction. Our results confirm an improvement in the reconstruction process. This will reduce the number of measurements needed in tomography, thus reducing the exposure to radiation in CT and increasing acquisition speed in MRI. The estimate of the parameter D in our optimality scheme is currently empirical. Designing an automated method for tuning D is an avenue for future work.

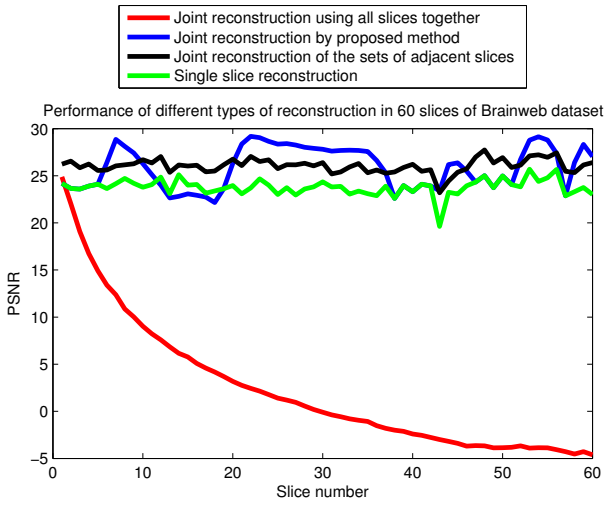

Figure 6: Reconstruction on the Brainweb dataset [1]. Our method combines slices (6-18), (20-37), (43-46), (52-56) and (58-60)

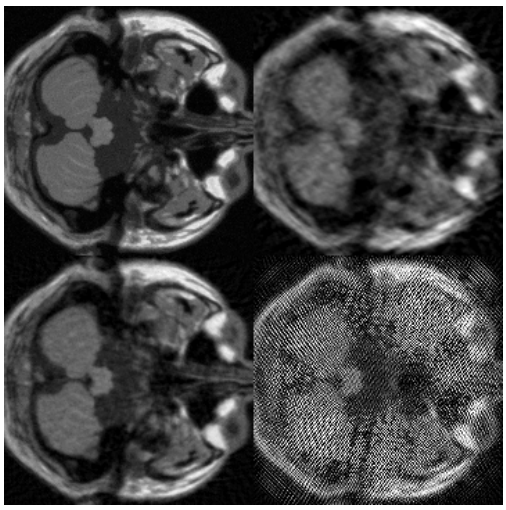

Figure 7: One of the reconstructed slices from Brainweb dataset [1]: Top left: original slice; top right: single slice reconstruction; bottom left: our method; bottom right: joint reconstruction of all slices together

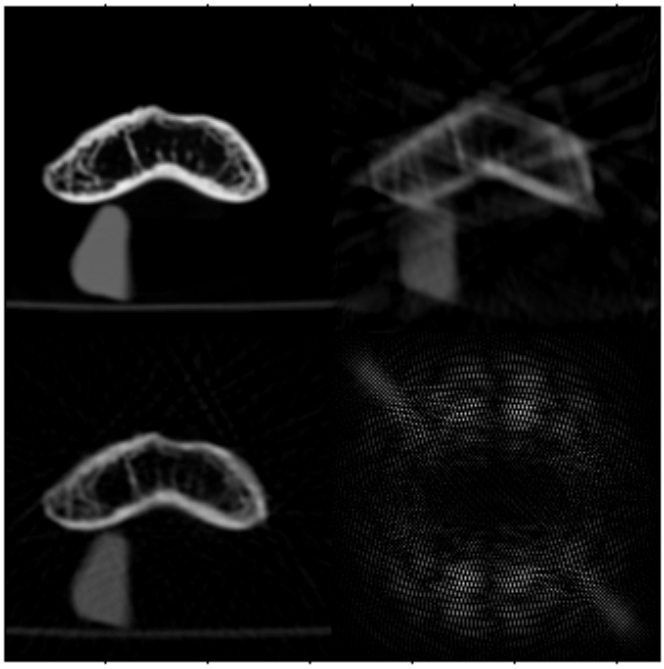

Figure 8: One of the reconstructed slices from Humerus dataset [2]: Top left: original slice; top right: single slice reconstruction; bottom left: our method; bottom right: joint reconstruction of all slices together

5. REFERENCES

[1] Brainweb MRI dataset. http://brainweb.bic.mni.mcgill.ca/brainweb/selection_normal.html, last viewed–July, 2016.

[2] Humerus CT dataset. http://isbweb.org/data/vsj/humeral/, last viewed–July, 2016.

[3] Lumbar MRI dataset. http://www.osirix-viewer.com/datasets/, last viewed–July, 2016.

[4] Walnut CT dataset. http://www.voreen.org/108-Data-Sets.html, last viewed–July, 2016.

[5] M. Asif, L. Hamilton, M. Brummer, and J. Romberg. Motion-adaptive spatio-temporal regularization for accelerated dynamic MRI. *Magnetic Resonance in Medicine*, 70(3):800–812, Sept. 2013.

[6] E. Candès and J. Romberg. Sparsity and incoherence in compressive sampling. *Inverse problems*, 23(3):969, 2007.

[7] E. Candès, J. Romberg, and T. Tao. Stable signal recovery from incomplete and inaccurate measurements. *Communications on pure and applied mathematics*, 59(8):1207–1223, 2006.

[8] D. Donoho. Compressed sensing. *IEEE Transactions on Information Theory*, 52(4):1289–1306, April 2006.

[9] S. Foucart and H. Rauhut. *A Mathematical Introduction to Compressive Sensing*. Birkhäuser Basel, 2013.

[10] R. C. Gonzalez and R. E. Woods. *Digital Image Procesing*. Pearson, third edition, 2009.

[11] A. K. Jain. *Fundamentals of Digital Image Procesing*. Prentice-Hall of India Pvt. Ltd., first edition, 1989.

[12] S.-J. Kim, K. Koh, M. Lustig, S. Boyd, and D. Gorinevsky. An interior-point method for large-scale l1-regularized least squares. *IEEE Journal of Selected Topics in Signal Processing*, 1(4):606–617, Dec 2007.

[13] J. Kleinberg and E. Tardos. *Algorithm Design*. Pearson, 2006.

[14] K. Koh, S.-J. Kim, and S. Boyd. l1-ls: Simple matlab solver for l1-regularized least squares problems.

https://stanford.edu/~boyd/l1_ls/, last viewed–July, 2016.

[15] W. Lu and N. Vaswani. Modified compressive sensing for real-time dynamic MR imaging. In *ICIP*, pages 3045–3048, Nov 2009.

[16] M. Lustig, D. Donoho, and J. Pauly. Sparse MRI: The application of compressed sensing for rapid MR imaging. *Magnetic Resonance in Medical Imaging*, 58(6):1182–1195, 2007.

[17] M. Lustig, J. Santos, D. Donoho, and J. Pauly. kt sparse: High frame rate dynamic MRI exploiting spatio-temporal sparsity. *Proceedings of the 13th Annual Meeting of ISMRM, Seattle*, 2006.

[18] R. F. Marcia, Z. Harmany, and R. Willett. Compressive coded aperture imaging. In *Proc. SPIE*, page 72460, 2009.

[19] T. Wang and T. Sze. The image moment method for the limited range CT image reconstruction and pattern recognition. *Pattern Recognition*, 34(11):2145–2154, 2001.